cells adequately in daily practice using an in vivo method: methodological and clinical considerations. *Eur J Nucl Med* 1995;22:61–67.
25. Altman DG. Some common problems in medical research, method comparison studies. In: Altman DG, ed. *Practical statistics for medical research*, 1st ed. London: Chapman and Hall; 1991:396–403.
26. Strauss HW, Griffeth LK, Shahrokh FD, et al. Cardiovascular system. In: Bernier DR, Christian PE, Laugan JK, eds. *Nuclear medicine technology and technics*, 3rd ed. St. Louis: Mosby Year Book; 1994:241–245.
27. Seawright SJ, Maton PJ, Greenall J. Factors affecting in vivo labeling of red blood cells. *J Nucl Med Technol* 1983;11:95.
28. Adalet I, Cantez S. Poor quality red blood cell labeling with technetium-99m: case report and review of the literature. *Eur J Nucl Med* 1994;21:173–175.
29. Rao SA, Knobel J, Collier BD, et al. Effect of Sn(II) ion concentration and heparin on technetium-99m red blood cell labeling. *J Nucl Med* 1986;27:1202–1206.
30. Sampson CB. Interference of patient medications in the radiolabelling of blood cells: in vivo and in vitro effects [Abstract]. *Eur J Nucl Med* 1994;21:S17.
31. Tatum JL, Burke TS, Hirsch JL, et al. Pitfall to modified in vivo method of technetium-99m red blood cell labeling: iodinated contrast media. *Clin Nucl Med* 1983;8:585–587.

Evaluation of Right and Left Ventricular Volume and Ejection Fraction Using a Mathematical Cardiac Torso Phantom

P. Hendrik Pretorius, Weishi Xia, Michael A. King, Benjamin M.W. Tsui, Tin-Su Pan and Bernard J. Villegas
Department of Nuclear Medicine, University of Massachusetts Medical Center, Worcester, Massachusetts; Department of Biomedical Engineering, University of North Carolina, Chapel Hill, North Carolina; and Department of Biophysics, University of the Orange Free State, Bloemfontein, South Africa

The availability of gated SPECT has increased the interest in the determination of volume and ejection fraction of the left ventricle (LV) for clinical diagnosis. However, the same indices for the right ventricle (RV) have been neglected. The objective of this investigation was to use a mathematical model of the anatomical distribution of activity in gated blood-pool imaging to evaluate the accuracy of two ventricular volume and ejection fraction determination methods. In this investigation, measurements from the RV were emphasized. **Methods:** The mathematical cardiac torso phantom, developed to study LV myocardium perfusion, was modified to simulate the radioactivity distribution of a ^{99m}Tc-gated blood-pool study. Twenty mathematical cardiac torso phantom models of the normal heart with different LV volumes (122.3 ± 11.0 ml), RV volumes (174.6 ± 22.3 ml) and stroke volumes (75.7 ± 3.3 ml) were randomly generated to simulate variations among patients. An analytical three-dimensional projector with attenuation and system response was used to generate SPECT projection sets, after which noise was added. The projections were simulated for 128 equidistant views in a 360° rotation mode. **Results:** The radius of rotation was varied between 24 and 28 cm to mimic such variation in patient acquisitions. The 180° and 360° projection sets were reconstructed using the filtered backprojection reconstruction algorithm with Butterworth filtering. Comparison was made with and without application of the iterative Chang attenuation correction algorithm. Volumes were calculated using a modified threshold and edge detection method (hybrid threshold), as well as a count-based method. A simple background correction procedure was used with both methods. **Conclusion:** Results indicate that cardiac functional parameters can be measured with reasonable accuracy using both methods. However, the count-based method had a larger bias than the hybrid threshold method when RV parameters were determined for 180° reconstruction without attenuation correction. This bias improved after attenuation correction. The count-based method also tended to overestimate the end systolic volume slightly. An improved background correction could possibly alleviate this bias.

Key Words: SPECT; ventricular volume; ejection fraction; gated blood-pool imaging

J Nucl Med 1997; 38:1528–1535

SPECT images can be used to determine left ventricular (LV) volume, ejection fraction (EF) and stroke volume (SV). There have been several investigations of LV function using gated SPECT (*1–6*). However, the same indices for the right ventricle (RV) have been neglected (*7*). The reasons for the LV emphasis are twofold (*8*). First, the LV is affected by many cardiovascular conditions before the RV is affected; and, second, its simple geometric shape (prolate ellipsoid) makes the LV easier to study than the complex quarter moon or crescent shape of the RV.

Several techniques have been used to determine ventricular volume in SPECT slices. Segmentation methods such as count threshold methods (*1,9–12*), count-based methods (*3,4*) and local gradient methods (*13*) have been used. In the count threshold method, voxels with counts higher than a predetermined threshold or fraction of the maximum count in the volume of interest (VOI) are included as part of the volume. The threshold is usually determined in phantom studies. The principle on which count-based methods are founded is that the total counts from all the activity within a VOI, irrespective of its location (in or outside the true edge), will be used in calculating the volume. This total count is then divided by the maximum count to obtain the number of voxels included in the VOI. Local gradient methods were frequently used for edge detection in planar gated blood pool studies. Both the threshold and count-based methods rely on a visual or global threshold to select the slices for inclusion in the three-dimensional volume determination. Two-dimensional local gradient methods that search for edges within two-dimensional slices are inaccurate because of the three-dimensional nature of the true boundary. Algorithms that perform in three dimensions provide more accurate determination of the actual edge locations, at the expense of increased algorithmic complexity (*10*).

When new methods or procedures are evaluated clinically, they are usually compared with a well-known and accurate gold standard. Inherent in any gold standard may be uncertainties and errors because of the assumptions made in the course of calculating the parameters of interest. The two major methods used to calculate LV and RV volume other than with emission imaging are x-ray angiography (*14,15*) and echocardiography (*16,17*). Each of these techniques has its own uncertainties. Accurate determination of the RV has been difficult because

Received Sep. 16, 1996; revision accepted Nov. 27, 1996.
For correspondence contact: P. Hendrik Pretorius, PhD, Department of Biophysics, University of the Orange Free State, P.O. Box 339 (G68), Bloemfontein, 9300, South Africa.
For reprints contact: Michael A. King, PhD, Department of Nuclear Medicine, University of Massachusetts Medical Center, 55 Lake Avenue North, Worcester, MA 01655.

TABLE 1
Patient Data

Patient no.	Sex	Size (cm)	ror (cm)	LV			RV			BF
				EDV	ESV	SV	EDV	ESV	SV	
1	F	36	26	123.3	48.5	74.8	191.3	114.3	77.0	lb
2	M	36	26	109.7	34.5	75.2	144.9	72.2	72.7	
3	F	36	24	115.0	34.7	80.3	179.9	102.7	77.2	sb, rl
4	M	40.4	28	124.1	52.2	71.9	151.0	77.0	74.0	fat, bg
5	F	36	25	140.6	67.9	72.7	147.0	70.4	76.6	sb, bg
6	F	36	25	109.6	29.4	80.2	207.8	132.3	75.5	lb, bg
7	M	36	25	130.8	52.9	77.9	163.6	84.5	79.1	
8	M	40.4	27	111.7	37.1	74.6	163.5	90.1	73.1	fat
9	F	36	26	122.5	44.1	78.4	174.4	96.3	78.1	sb
10	M	36	24	107.7	29.5	78.2	197.7	123.7	74.0	
11	F	36	24	106.0	25.9	80.1	211.4	137.4	74.0	sb, rl
12	F	36	25	118.3	47.4	70.9	198.1	123.8	74.3	sb, rl
13	M	40.4	27	113.8	40.0	73.8	200.7	126.2	74.5	fat
14	M	36	24	117.4	39.3	78.1	182.6	105.6	77.0	
15	F	36	26	142.1	69.0	73.1	177.0	97.9	79.1	lb
16	M	40.4	27	124.1	47.7	76.4	171.5	94.1	77.4	fat
17	M	36	27	133.4	62.3	71.1	152.8	77.7	75.1	
18	F	36	28	128.6	48.4	80.2	152.2	72.8	79.4	lb, rl
19	M	40.4	28	133.4	59.6	73.8	138.9	63.3	75.6	fat
20	F	36	28	133.9	62.7	71.2	186.0	108.7	77.3	lb
Average				122.3	46.7	75.7	174.6	98.6	76.1	

ror = radius of rotation; BF = body factors; lb = large breasts; sb = small breasts; rl = raised liver; fat = 2.2 cm of fat added; bg = elevated background (15%–20%, compared to 10%).

angiography and echocardiography require highly detailed assumptions about the RV's geometry (*8,14–17*). Magnetic resonance imaging (*8,18,19*) and ultrafast CT (*20,21*) are also becoming accurate modalities for heart volume calculation, with the latter being the method of choice. Phantom studies are useful to validate new techniques. The major advantage of phantom experiments is that they allow control over variables and provide knowledge about parameters to be measured. The major disadvantage of phantom experiments has been their lack of clinical applicability because of oversimplification of the anatomy.

The objective of this investigation was to use a mathematical model that realistically simulates the normal anatomy of the human torso with an activity distribution that models gated blood pool imaging to evaluate the accuracy of two methods that can be used to determine the ventricular volumes and EFs. In this investigation, determination of the volumes and parameters of the RV was emphasized.

MATERIALS AND METHODS

Phantom Design

The mathematical cardiac torso phantom (MCAT) developed for myocardial SPECT studies (*22,23*) was modified to allow investigation of cardiac function (*24,25*). The MCAT phantom uses simple geometric representations (ellipsoids and cylinders) to model the normal heart, other organs and body outline. It originated from the reference human developed for internal dosimetery purposes (*26*) and was modified to better approximate the dimensions and shapes of the organs for imaging purposes (*27*). The shape, volume and mass of the LV and RV were derived from various sources (*2,19,21,26–30*). In this study, the model was further extended to include 16 different time frames to represent the motion of the heart during the heart cycle using a volume curve from Guyton (*28*). For planar gated blood-pool imaging, Bacharach et al. (*31*) determined that frame intervals of 50 msec per frame at rest and 40 msec per frame during exercise were sufficient for measurement of EF. Similarly, Van Aswegen et al. (*32*) found that 16 time frames were adequate to determine EF but not parameters such as peak filling and ejection rate. It is general practice to acquire 8–16 time frames with gated SPECT due to statistical, computational and disk space considerations (*1–6*). Thus, 16 time frames were used in this investigation. The LV and RV volumes (*19,26,30*) and myocardium thickness (*2,21*) were modified for improved agreement with typical human anatomy and to include conservation of myocardial mass during a beating cycle of the heart. A radioactivity distribution that simulated a ^{99m}Tc-gated blood-pool study was simulated; that is, the major concentration of activity was within the chambers of the heart (ventricles and atria), and a background level of 10%–20% of the heart concentration was used in the phantom.

To simulate the variability that is present in clinical situations, 20 MCAT models of the normal heart with different LV and RV volumes and SVs were generated within a normal range of variations from the normal average model (Table 1). This was accomplished using the assumption that the fraction of the ellipsoids used to simulate any given ventricle is a constant, regardless of the change in volume. Therefore, these fractions for the average model were calculated and applied to the randomly generated volumes, taking into account the change in SV. In this way, 16 different time frames (volume curve) for the 20 MCAT hearts were generated. To further enhance mimicking clinical variability, a patient population consisting of 10 men and 10 women with four different torso sizes (Table 1), namely, a 36-cm male torso, a 36-cm female torso with small breast, a 36-cm female torso with large breast and a 36-cm male torso with 2.2 cm of fat added (40.4 cm in total), were simulated. The torso size was the maximum lateral width of the phantom. In some patients, the liver was raised such that a portion of it was contained within the slices of the heart.

Data Simulation, Reconstruction and Analysis

An analytical three-dimensional projector with attenuation and detector response included was used to generate the projection

TABLE 2
Predetermined Threshold Values Used in the Hybrid Threshold Method

Reconstruction strategy	LV (%)	RV (%)
180°, without attenuation	40	37
180°, Chang attenuation	43	41
360°, with attenuation	47	42
360°, Chang attenuation	48	44

datasets (*33*). Poisson noise was added based on an average total projection counts of 12.5 million at diastole (~97,600 counts per projection image). The contribution of scatter was not considered in this study; that is, perfect scatter correction was assumed. In practice, one of several different scatter compensation methods (*34–38*) could be used to correct for scatter. Correction for scatter by one of the scatter subtraction methods would lead to an increased image noise level and thus may have an impact on the accuracy of edge definition. This issue deserves consideration; however, the time to run Monte Carlo simulation of the large number of three-dimensional datasets included in this investigation was prohibitive. The simulated SPECT system was based on a commercial system with a low-energy, high-resolution (LEHR) collimator. The pixel size was 0.317 cm. SPECT projections were simulated in 128 equidistant views in a 360° rotation mode. The radius of rotation was varied between 24 and 28 cm to realistically simulate patient setup procedures in the clinic (Table 1). Data were reconstructed using filtered backprojection reconstruction with Butterworth filtering, with a cutoff frequency of 0.625 cycles/cm and an order of 4. Data were reconstructed using different reconstruction strategies: using all the data acquired through 360° without attenuation correction; using 180° data (45° RAO to 45° LPO) without attenuation correction; using all the data acquired through 360° with one iteration of Chang attenuation correction (*39*); and using 180° data with one iteration of Chang attenuation correction. Transverse slices were reformatted to horizontal long axis slices and background corrected using a region of interest (ROI) adjacent to the LV.

Two different methods were used to determine the ventricular volume. First, a simple hybrid count threshold (hybrid threshold) method was used. The average maximum count in the ventricle of interest was determined using a 5 × 5 pixel region around the maximum. The average maximum count was used instead of the maximum because of the noisy nature of the data. The number of slices was selected using a predetermined threshold value. The threshold value for each data set was calibrated using the end diastolic volumes (EDVs) of all phantom patients and varied between 37% and 48% (Table 2). This was done to investigate if there was a need for a variable threshold value as the volume decreased, as suggested by Faber et al. (*2*). The threshold for each phantom patient was determined by changing the fractional value until the true volume was obtained within a high accuracy. The threshold value that gave the best overall results for all phantom patients was chosen as the predetermined threshold value. The center of mass of the ventricle was calculated, and a search pattern from that location radially outward was instituted. The search was constrained by a manually drawn ROI on the diastole time frame. A local gradient (first derivative) was calculated and used in combination with the threshold to find the edge of the ventricle in each slice. The edge was selected either by the maximum gradient between the center of mass and the manually drawn ROI or the count threshold, depending upon which was reached first.

The second method was a count-based volume quantitation technique. As with the threshold method, the center of mass was found, a search radially outward was launched and the maximum gradient was used to determine the edge. The ROI found in this way was dilated to include two additional voxels in all directions, in an effort to include all the activity (counts) belonging to the VOI (blurred into the surroundings). In this method, the number of slices consists of that used in the threshold method, as well as two additional slices on both sides. All the counts included were summed and divided by the average maximum count. This yielded the estimate of the number of voxels included in the VOI.

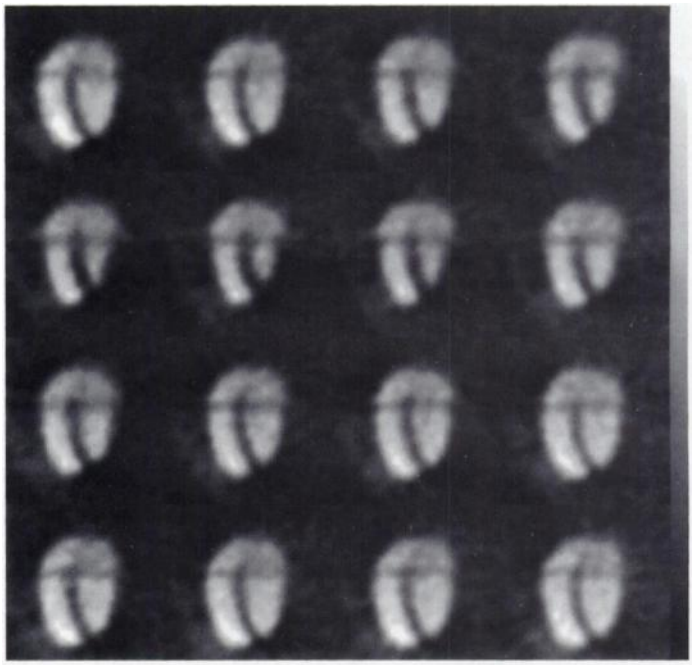

FIGURE 1. Horizontal long-axis images of a gated SPECT blood-pool phantom patient without attenuation correction. The images consist of 16 time frames from one slice through the center of the ventricles during the cardiac cycle, reconstructed using 180° data.

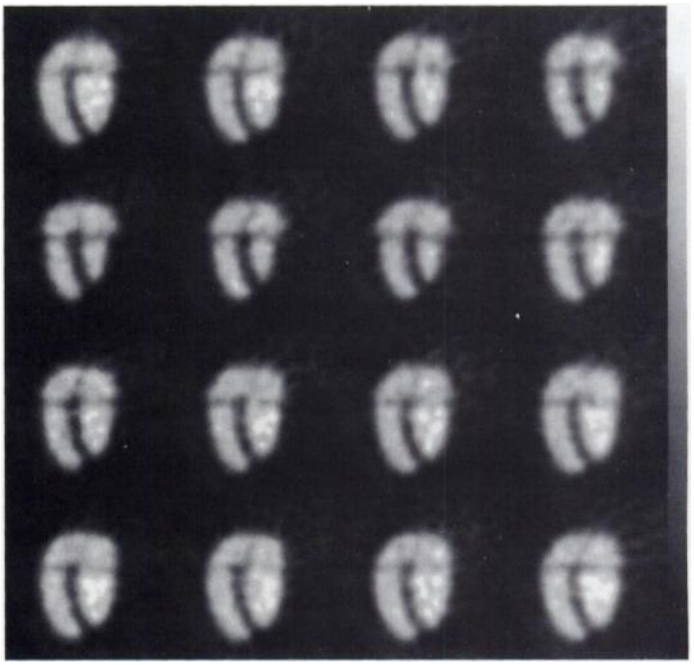

FIGURE 2. Horizontal long-axis images of a gated SPECT blood-pool phantom patient with attenuation correction. The images consist of 16 time frames from one slice through the center of the ventricles during the cardiac cycle, reconstructed using 180° data.

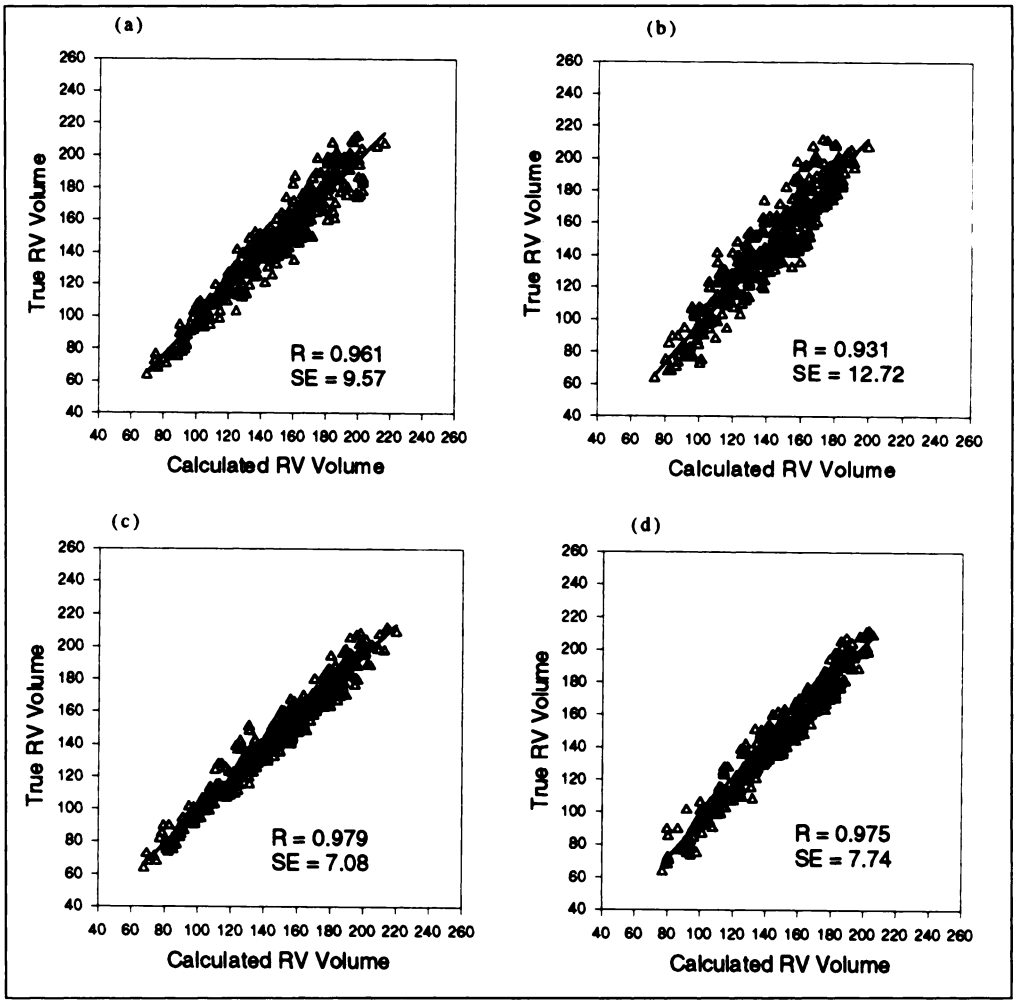

FIGURE 3. Regression curves comparing calculated RV volumes without attenuation correction with the true volumes: (a) 180° hybrid threshold method, (b) 180° count-based method, (c) 360° hybrid threshold method and (d) 360° count-based method.

Statistical Analysis

Linear regression analysis (*40*) was done using all calculated volumes for the RV and LV compared to the true volumes for the respective ventricles. Regression values (r) and standard errors of the estimate (s.e.) were calculated as an indication of performance of the two methods investigated.

RESULTS

In Figures 1 and 2, horizontal long-axis images of a gated SPECT blood-pool phantom patient without and with attenuation correction, respectively, are given. The images consist of 16 time frames from one slice through the center of the ventricles during the cardiac cycle, reconstructed using 180° data. The improvement in contrast and uniformity of the distribution of activity within the ventricles are clearly visible for the attenuation corrected image set. The latter was especially true for the RV.

In Figures 3 and 4, the results from the regression analysis for the RV are given. In both figures, a and b represent the results from the 180° projection data, whereas c and d represent the results from the 360° projection data. Furthermore, a and c are the results obtained using the hybrid threshold method, whereas b and d are the results using the count-based method. Figure 3 summarizes the regression analysis for the RV volumes reconstructed without attenuation correction. Excellent correlations were obtained that varied between 0.931 and 0.979, whereas the s.e. values varied between 7.1 and 12.7 ml. The spread of the volumes around the regression line is noticeably better for the 360° case (smaller s.e.). In Figure 4, the regression results

TABLE 3
Results in Terms of Measured Value Divided by True Value of the Parameter Using 180° and 360° Projections without Attenuation Correction

	EDV		ESV		SV		EF	
	360°	180°	360°	180°	360°	180°	360°	180°
LV, hybrid threshold	0.976	0.988	0.990	0.965	0.970	1.002	0.994	1.013
	(0.044)	(0.052)	(0.080)	(0.097)	(0.061)	(0.079)	(0.042)	(0.045)
LV, count-based	0.984	0.977	1.116	1.119	0.914	0.907	0.929	0.928
	(0.051)	(0.073)	(0.134)	(0.170)	(0.068)	(0.092)	(0.048)	(0.059)
RV, hybrid threshold	(1.030)	1.017	1.020	1.048	1.045	0.983	1.014	0.965
	0.065	(0.065)	(0.060)	(0.070)	(0.071)	(0.097)	(0.058)	(0.054)
RV, count-based	1.003	(0.961)	1.074	1.047	0.921	0.864	0.918	0.900
	(0.041)	0.077	(0.088)	(0.127)	(0.095)	(0.086)	(0.082)	(0.075)

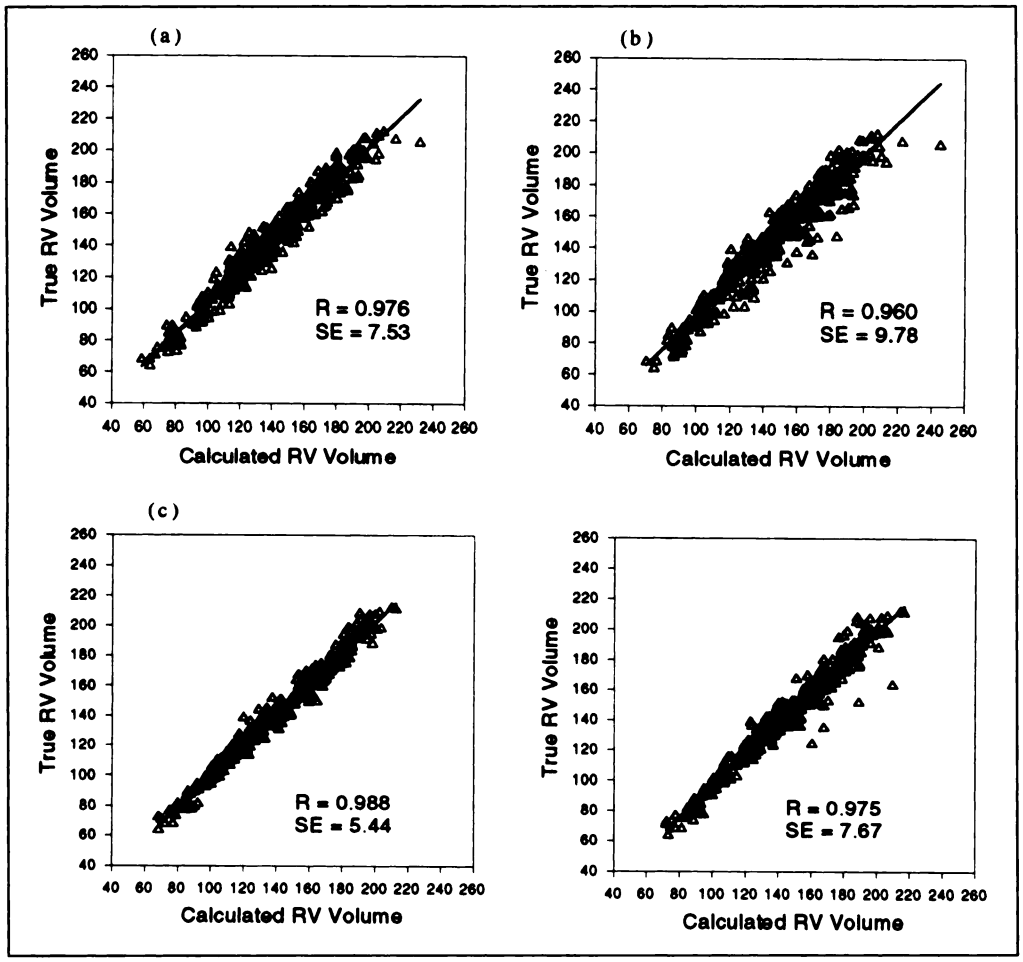

FIGURE 4. Regression curves comparing calculated RV volumes with iterative Chang attenuation correction with the true volumes: (a) 180° hybrid threshold method, b) 180° count-based method, (c) 360° hybrid threshold method and (d) 360° count-based method.

obtained with attenuation corrected RV data are given. The regression values varied between 0.960 and 0.988, and the s.e. values varied between 5.44 and 9.78 ml. Note the decrease in the s.e. for attenuation-corrected data compared to data without attenuation correction (Fig. 3 versus Fig. 4).

Regression results for the LV volumes without attenuation correction varied between 0.967 and 0.984, whereas the s.e. values varied between 5.3 and 7.7 ml. The same parameters varied between 0.978 and 0.991 and 4.04 and 6.21 ml, respectively, when attenuation correction was applied.

Figures 5 and 6 compare the calculated average RV and LV volume curves with that of the phantom over a cardiac cycle. The lines represent the true values derived from the phantom, whereas the symbols represent the calculated values. The s.d. values for the different volume curves are not shown but were about ±12.0 ml for the LV and ±22.0 ml for the RV for both datasets. In both Figures 5 and 6, a and b represent the results from the 180° projection data, whereas c and d are the results from the 360° projection data. Furthermore, a and c are results obtained using the hybrid threshold method, whereas b and d are results using the count-based method. The hybrid threshold method performed satisfactorily, as indicated by the similarities between the lines and the symbols in all the figures. The count-based method tends to slightly overestimate the end systolic volume (ESV) for all cases (Figs. 5 and 6, b and d) and perform unsatisfactorily in the case of 180° projection data with no attenuation correction (Fig. 5b), although the regression coefficient (r = 0.931) is still excellent. Improvement was apparent after attenuation correction (Fig. 6b).

Tables 3 and 4 give the results of measured parameters (EDV, ESV, SV and EF) as fractions of the true parameter values. The values calculated for each parameter with each method are an indication of the bias (closer to 1.0 for less bias), and the s.d. values are an indication of the variability (precision) of the methods. In Table 3, the results for parameters obtained using 360° and 180° projection data without attenuation correction are summarized. The bias in the calculated parameters for 360° projection data varied between −2.4 and 3.0%, −1.0 and 11.6%, −8.6 and 4.5% and −8.2 and 1.4% for EDV, ESV, SV and EF, respectively. The count-based method performed the worst for both ventricles, and this decreased performance is especially visible in the parameters derived from volume calculation (SV and EF). In all cases, the results for 180° projection data were comparable to that of the 360° projection data. These results once again demonstrate the effect of the overestimation of the ESV using the count-based method. In Table 4, results obtained using the Chang attenuation correction method are given for 360° and 180° projection data. Results for the count-based with attenuation correction show improved accuracy over those without attenuation correction, whereas for the hybrid threshold method, the results obtained from with and without attenuation correction are comparable. Comparing Figures 1 and 2, the improvement in the quantitative results of the count-based method coincide with the visual improvement in contrast and uniformity after attenuation correction.

DISCUSSION

Our results indicate that cardiac functional parameters can be measured with reasonable accuracy, with both the hybrid threshold and the count-based methods. Both methods are fast and easy to implement. The disadvantage of the count threshold edge detection technique is the need to calibrate (to adapt the

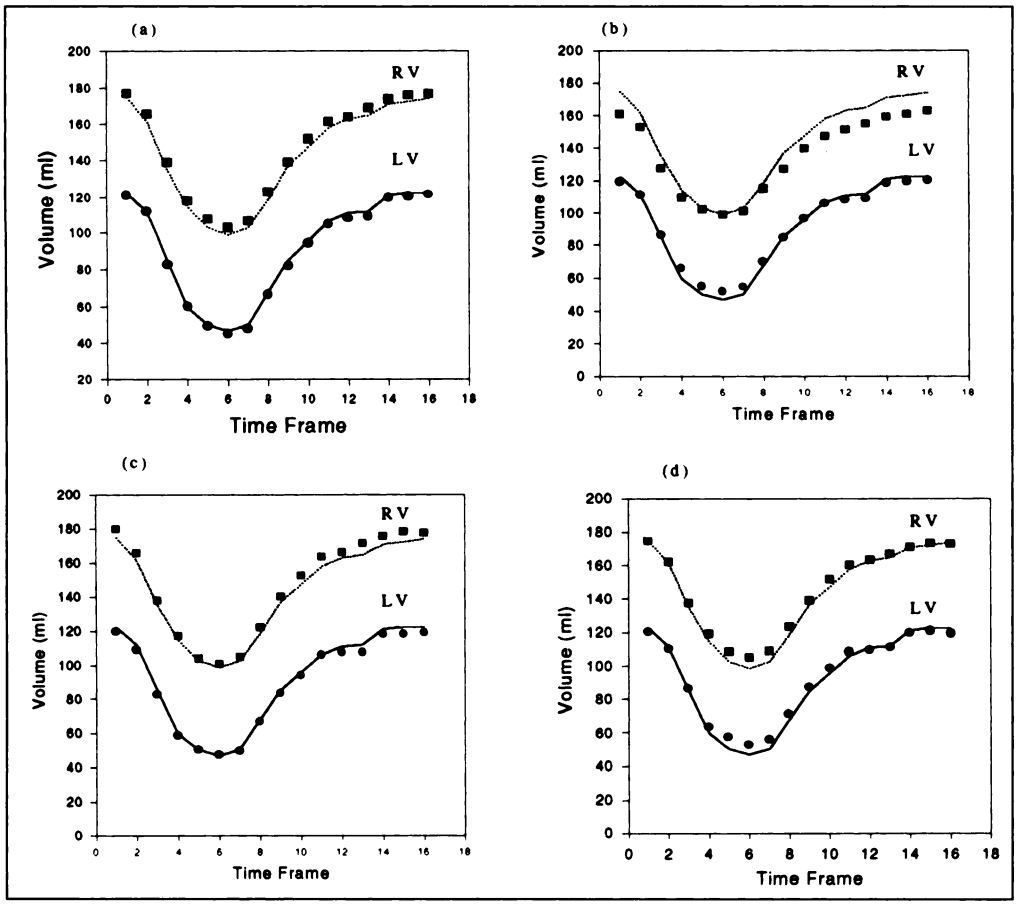

FIGURE 5. Comparison of true LV and true RV volume with the calculated volumes without attenuation correction. The solid lines represent the true values, whereas the symbols represent the calculated average values. (a) 180° hybrid threshold method, (b) 180° count-based method, (c) 360° hybrid threshold method and (d) 360° count-based method.

threshold) for each reconstruction strategy, as indicated by the differences in percent threshold in Table 2. The count-based method consistently overestimates ESV slightly (between 4.6 and 12.7%) for both the ventricles. This is probably due to its inability to accurately correct for the contribution of background using the ROI adjacent to the LV, and improved methods of background correction are desirable.

The need to change the count threshold between the EDV and ESV calculation, as suggested by Faber et al. (*2*), was not observed in the simulation studies investigated herein. This is

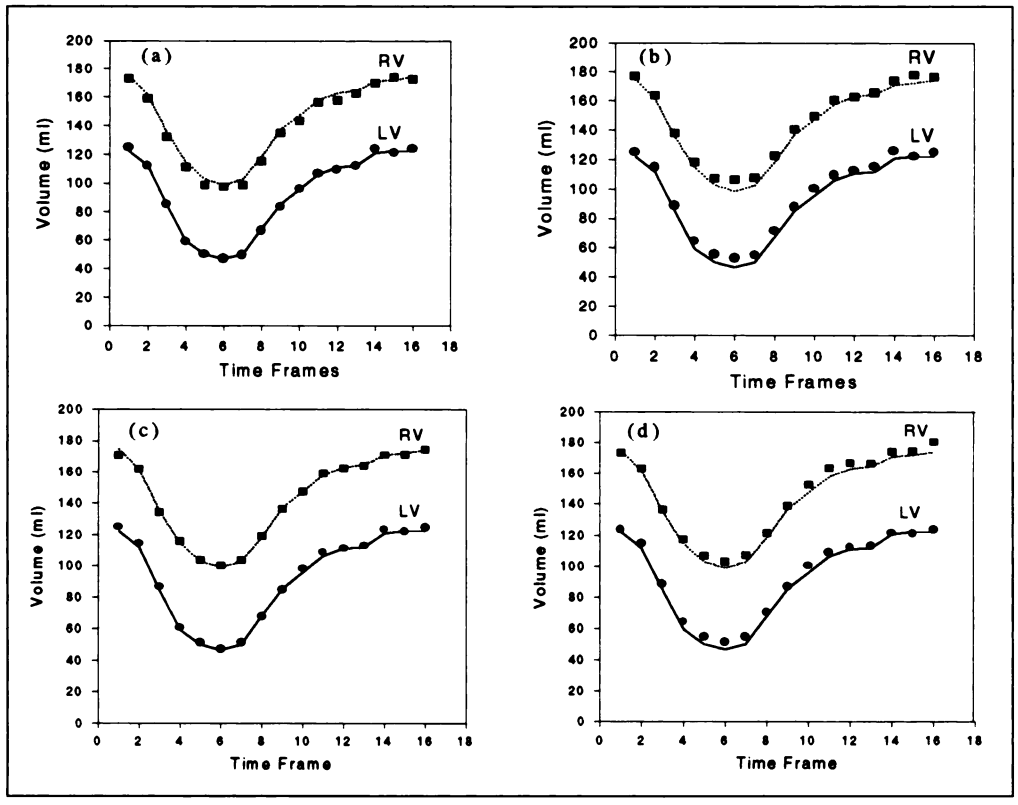

FIGURE 6. Comparison of true LV and true RV volume with the calculated volumes using one iteration of Chang attenuation correction. The solid lines represent the true values, whereas the symbols represent the calculated average values. (a) 180° hybrid threshold method, (b) 180° count-based method, (c) 360° hybrid threshold method and (d) 360° count-based method.

TABLE 4
Results in Terms of Measured Value Divided by True Value of the Parameter Using the 360° and 180° Projections with Chang Attenuation Correction (One Iteration)

	EDV		ESV		SV		EF	
	360°	180°	360°	180°	360°	180°	360°	180°
LV, hybrid threshold	1.020	1.012	1.017	1.001	1.028	1.033	1.007	1.015
	(0.042)	(0.057)	(0.061)	(0.073)	(0.063)	(0.078)	(0.034)	(0.037)
LV, count-based	1.012	1.023	1.108	1.127	0.967	0.976	0.955	0.954
	(0.051)	(0.050)	(0.110)	(0.136)	(0.074)	(0.072)	(0.045)	(0.050)
RV, hybrid threshold	0.979	0.992	1.010	0.978	0.945	1.016	0.965	1.025
	(0.030)	(0.033)	(0.046)	(0.058)	(0.069)	(0.063)	(0.054)	(0.060)
RV, count-based	0.994	1.020	1.046	1.076	0.939	0.961	0.943	0.941
	(0.036)	(0.082)	(0.067)	(0.095)	(0.091)	(0.113)	(0.073)	(0.088)

because of the use of a local gradient in conjunction with a global threshold. At end diastole, the separation between the ventricular chambers is at its minimum (myocardium at its thinnest), and the partial volume effect impact on the separation (myocardium) is at its peak. A higher threshold is needed (if not used with a local gradient) to separate the ventricles. In end systole, the separation is at its maximum (the partial volume effect at its minimum), and a lowerthreshold is needed. In this study, the incorporation of a local gradient eliminates the need to change the threshold value between diastole and systole.

A comparison of 180° versus 360° reconstructions shows that the hybrid threshold method has similar accuracies with both reconstruction strategies. The reason for this is the calibration of the predetermined threshold value for each method (Table 2). The count-based method was more accurate after application of one iteration of Chang's attenuation correction method. This is especially true for the RV (compare Fig. 5b with Fig. 6b and Tables 3–4). The attenuation correction method was able to reduce the distortion of counts, which was more prominent in case of the RV due to its more superficial location. In clinical practice, it should be possible to implement the count-based method without the added complication of calibration for the specific camera system and imaging protocol. In combination with attenuation correction, 180° projection data could be used to save time and disk space.

A limitation of the use of the MCAT model is that the structure of the RV and LV is represented by smooth geometric shapes. This may have made the segmentation task easier because the detailed structure of the ventricles is not modeled. The finite spatial resolution inherent in SPECT imaging does, however, decrease the impact of this deficiency. The influence of the motion of the valvular plane was not studied during this investigation and could have an effect on the overall accuracy of the method in a clinical environment. Presently in the MCAT phantom, the valvular planes are assumed to be stationary during the cardiac cycle. Patient motion (physical and respiratory) can also be an influencing factor, and studies should be performed to investigate the extent of such influences. The heart model of the MCAT phantom can be further modified to realistically represent the motion of the valvular plane, motion within every time frame to include the influence of the finite temporal resolution and details of structure, such as inclusion of papillary muscles. Larger diastolic volumes (>211.4 ml for the RV and 142.1 for the LV) can also be studied to verify volume calculation methods herein. However, previous investigations with phantoms (*10,12*) have showed that more variation in the percent threshold is possible at smaller volumes. Thus, it is at the smaller volumes that the accuracy of volume quantitation is most challenged. In this study, the smallest volume simulated was 25.9 ml at LV end systole.

CONCLUSION

The results indicate that cardiac functional parameters can be measured with reasonable accuracy using both methods with gated SPECT blood-pool imaging. However, the count-based method had a larger bias than the hybrid threshold method in determining RV parameters for 180° reconstruction without attenuation correction. This bias improved after attenuation correction. Thus, the used of attenuation correction with count-based volume quantitation for the RV is recommended. The count-based method also tended to overestimate the ESV slightly. An improved background correction could possibly alleviate this bias.

ACKNOWLEDGMENTS

This publication was made possible by grant HL-50349 from the National Heart, Lung and Blood Institute, and its contents are solely the responsibility of the authors and do not necessarily represent the official views of the National Heart, Lung and Blood Institute. We also thank the Foundation for Research and Development of South Africa, the Faculty of Medicine and the Biophysics Department of the University of the Orange Free State, Bloemfontein, South Africa, for financial support during P. Hendrik Pretorius's postdoctoral fellowship at the University of Massachusetts Medical Center, Worcester, MA.

REFERENCES

1. Corbett JR, Jansen DE, Lewis SE, et al. Tomographic gated blood pool radionuclide ventriculography: analysis of wall motion and left ventricular volumes in patients with coronary artery disease. *J Am Coll Cardiol* 1985;6:349–358.
2. Faber TL, Stokely EM, Templeton GH, Akers SM, Parkey RW, Corbett JR. Quantification of three-dimensional left ventricular segmental wall motion and volumes from gated tomographic radionuclide ventriculograms. *J Nucl Med* 1989;30: 638–649.
3. Bunker SR, Hartshome MF, Scmidt WP, et al. Left ventricular volume determination from single-photon emission computed tomography. *Am J Roentgenol* 1985;144:295–298.
4. Caputo GR, Graham M, Brust KD, Kennedy JW, Nelp WB. Measurement of left ventricular volume using single-photon emission computed tomography. *Am J Cardiol* 1985;56:781–786.
5. Underwood SR, Walton S, Laming PJ, Jarritt PJ, Ell PJ. Left ventricular volume and ejection fraction determined by gated blood pool emission tomography. *Br Heart J* 1985;53:216–222.
6. Aurigemma GP, Gaasch WH, Villegas B, Meyer TE. Noninvasive assessment of left ventricular mass, chamber volume and contractile function. *Curr Probl Cardiol* 1995;20:361–440.
7. Corbett JR. Tomographic radionuclide ventriculography: opportunity ignored? *J Nucl Cardiol* 1994;1:567–570.
8. Katz J, Whang J, Boxt LM, Barst RJ. Estimation of right ventricular mass in normal subjects and in patients with primary pulmonary hypertension by nuclear magnetic resonance imaging. *J Am Coll Cardiol* 1993;21:1475–1481.
9. Jang S, Jaszczak RJ, Li J, et al. Cardiac ejection fraction and volume measurements using dynamic cardiac phantoms and radionuclide imaging. *IEEE Trans Nucl Sci* 1994:2845–2849.
10. Long DT, King MA, Sheehan J. Comparative evaluation of image segmentation methods for volume quantitation in SPECT. *Med Phys* 1992;19:483–489.
11. Pretorius PH, Van Aswegen A, Lötter MG, Herbst CP, Nel MG, Otto AC. Verification of a varying threshold edge detection SPECT technique for spleen volume: a comparison with computed tomography volumes. *J Nucl Med* 1993;34:963–967.

12. Pretorius PH, Van Aswegen A, Herbst CP, Lötter MG. The effects of different correction techniques on absolute volume determination with SPECT using a threshold edge detection method. *Med Phys* 1991;18:390–393.
13. Nelson AD, Muswick GJ, Muzic RF, Deschamps X. A robust edge detection method for gated radionuclide ventriculograms. *J Nucl Med* 1996;37:685–689.
14. Arcilla RA, Tsai P, Thilenius O, Ranniger K. Angiocardiographic method for volume estimation of right and left ventricle. *Chest* 1971;60:446–454.
15. Gentzler RD, Briselli MF, Gault JH. Angiographic estimation of right ventricular volume in man. *Circulation* 1974;50:324–330.
16. Starling MR, Crawford MH, Sorensen SG, O'Rouke RA. A new two-dimensional echocardiographic technique for evaluating right ventricular size and performance in patients with obstructive lung disease. *Circulation* 1982;66:612–620.
17. Bommer W, Weinert L, Neumann A, Neef J, Mason DT, DeMaria A. Determination of right atrial and right ventricular size by two-dimensional echocardiography. *Circulation* 1979;60:91–100.
18. Boxt LM, Katz J, Kolb T, Barst RJ. Direct quantitation of right and left ventricular volumes using magnetic resonance imaging in patients with pulmonary hypertension. *J Am Coll Cardiol* 1992;19:1508–1515.
19. Benjelloun H, Cranney GB, Kirk KA, Blackwell GG, Lotan CS, Pohost GM. Interstudy reproducibility of biplane cine nuclear magnetic resonance measurements of left ventricular function. *Am J Cardiol* 67:1413–1420.
20. Reiter SJ, Rumberger JA, Feiring AJ, Stanford W, Marcus ML. Precision of measurements of right and left ventricular volume by cine computed tomography. *Circulation* 1986;74:890–900.
21. Hajduczok ZD, Weiss RM, Stanford W, Marcus ML. Determination of right ventricular mass in human and dogs with ultrafast computed tomography. *Circulation* 1990;82:202–212.
22. Terry JA. A receiver operating analysis of parallel, fan beam and cone beam collimator designs for cardiac single photon emission computed tomography imaging [PhD dissertation]. Chapel Hill, NC: University of North Carolina, 1992.
23. Tsui BMW, Zhoa XD, Gregoriou GK, et al. Quantitative cardiac SPECT reconstruction with reduced image degradation due to patient anatomy. *IEEE Trans Nucl Sci* 1994;41:2838–2844.
24. Xia W, Tsui BMW, King MA, Villegas BJ. Cardiac motion simulation and study of its influence on the polar map of the left ventricular wall [Abstract]. *J Nucl Med* 1995;36:59P.
25. Pretorius PH, Xia W, King MA, Tsui BMW, Pan T-S, Villegas BJ. Determination of left and right ventricular volume and ejection fraction using a mathematical cardiac torso phantom for gated blood pool SPECT [Abstract]. *J Nucl Med* 1996;37:97P.
26. Snyder WS, Cook MJ, Nasset ES, Karhausen LR, Howells GP, Tipton IH. Report of the task group on the reference man. ICRP Series 23, 1974.
27. Coffey JL. A revised mathematical model of the heart for use in radiation absorbed dose calculation [MS dissertation]. Knoxville, TN: University of Tennessee, 1978.
28. Guyton AC. *Textbook of medical physiology*, 7th ed. Philadelphia: WB Saunders; 1986:150–164.
29. Weyman AE. *Principles and practices of echocardiography*, 2nd ed. Philadelphia: Waverly; 1994:1290–1294.
30. Yang SS, Bentivoglio LG. *From cardiac catheterization data to hemodynamic parameters*, 3rd ed. Philadelphia: FA Davis; 1988:102–105.
31. Bacharach SL, Green MV, Borer JS, Hyde JE, Farkas SP, Johnston GS. Left-ventricle peak ejection rate, filling rate and ejection fraction: frame rate requirements at rest and exercise. *J Nucl Med* 1979;20:189–193.
32. Van Aswegen A, Alderson PO, Nickoloff EL, Housholder DF, Wagner HN Jr. Temporal resolution requirements for left ventricular time–activity curves. *Radiology* 1980;135:165–170.
33. Pan T-S, Luo D-S, King MA. Design of an efficient three-dimensional projector and backprojector pair for SPECT. In: *Proceedings of fully three-dimensional image reconstruction in radiology and nuclear medicine*. Aix-les-Bains, Savorie, France 1995:181–185.
34. King MA, Hademenos GJ, Glick SJ. A dual-photopeak window method for scatter correction. *J Nucl Med* 1992;33:605–612.
35. Pretorius PH, Van Rensburg AJ, Van Aswegen A, Lötter MG, Serfontein DE, Herbst CP. The channel ratio method of scatter correction for radionuclide image quantitation. *J Nucl Med* 1993;34:330–335.
36. Jaszczak RJ, Greer KL, Floyd CE Jr, Harris CC, Coleman RE. Improved SPECT quantitation using compensation for scattered photons. *J Nucl Med* 1984;25:893–900.
37. Axelsson B, Msaki P, Israelsson A. Subtraction of compton-scattered photons in single-photon emission computerized tomography. *J Nucl Med* 1984;25:490–494.
38. Ichihara T, Ogawa K, Motomura N, Kubo A, Hashimoto S. Compton scatter compensation using the triple-energy window method for single- and dual-isotope SPECT. *J Nucl Med* 1993;34:2216–2221.
39. Chang LT. A method for attenuation correction in radionuclide computed tomography. *IEEE Trans Nucl Sci* 1978;25:638–643.
40. Pollard JH. *A handbook of numerical and statistical techniques*. Cambridge, UK: Cambridge University Press; 1979:161–163.

Myocardial Perfusion Imaging with a Combined X-Ray CT and SPECT System

Kathrin Kalki, Stephen C. Blankespoor, J. Keenan Brown, Bruce H. Hasegawa, Michael W. Dae, Michael Chin and Carol Stillson

UCSF Physics Research Laboratory, Department of Radiology, Bioengineering Graduate Group and Cardiovascular Research Institute, University of California San Francisco, San Francisco, California

We evaluated a novel combined x-ray CT and SPECT medical imaging system for quantitative in vivo measurements of ^{99m}Tc-sestamibi uptake in an animal model of myocardial perfusion. **Methods:** Correlated emission-transmission myocardial images were obtained from 7- to 10-kg pigs. The x-ray CT image was used to generate an object-specific attenuation map that was incorporated into an iterative ML-EM algorithm for reconstruction and attenuation correction of the coregistered SPECT images. The pixel intensities in the SPECT images were calibrated in units of radionuclide concentrations (MBq/g), then compared against in vitro ^{99m}Tc activity concentration measured from the excised myocardium. In addition, the coregistered x-ray CT image was used to determine anatomical boundaries for quantitation of myocardial regions with low perfusion. **Results:** The accuracy of the quantitative measurement of in vivo activity concentration in the porcine myocardium was improved by object-specific attenuation correction. However, an additional correction for partial volume errors was required to retrieve the true activity concentration from the reconstructed SPECT images. **Conclusion:** Accurate absolute SPECT quantitation required object-specific correction for attenuation and partial volume effects. Additional anatomical information from the x-ray CT image was helpful in defining regions of interest for quantitation of the SPECT images.

Key Words: SPECT; quantification; myocardial perfusion; image coregistration

J Nucl Med 1997; 38:1535–1540

Absolute quantitation of radionuclide uptake from SPECT is compromised by photon attenuation, scattered radiation and partial volume errors (*1,2*). Therefore, several investigators have incorporated transmission measurements into reconstruction of the radionuclide image for compensation of photon attenuation. SPECT images also have been coregistered with images from x-ray CT or MRI (*3,4*) to improve anatomical definition, localization and quantitative accuracy of functional information obtained with SPECT.

We are developing a new imaging device, christened the emission-transmission CT (ETCT) system, which uses a common detector and imaging geometry to obtain a co-registered functional data from SPECT and anatomical data from x-ray CT. For quantitative measurements, the transmission CT image can be used to generate an object-specific attenuation map for attenuation compensation of the SPECT data. In this study we

Received Nov. 10, 1995; revision accepted Sep. 11, 1996.

For correspondence or reprints contact: Bruce Hasegawa, PhD, UCSF Physics Research Laboratory, 389 Oyster Point Blvd., Suite 1, So., San Francisco, CA 94080.